Influence of the Number of Nanoparticles on the Enhancement Properties of Surface-Enhanced Raman Scattering Active Area: Sensitivity *versus* Repeatability

Jérémie Margueritat,[†,‡,*] Hélène Gehan,[§] Johan Grand,[§] Georges Lévi,[§] Jean Aubard,[§] Nordin Félidj,[§] Alexandre Bouhelier,[‡] Gerard Colas-Des-Francs,[‡] Laurent Markey,[‡] Carmen Marco De Lucas,[‡] Alain Dereux,[‡] and Eric Finot[‡]

[†]Interfaces, Traitements, Organisations et Dynamique des Systèmes, Université Paris7-Denis Diderot, UMR 7086, Bâtiment Lavoisier, 15 rue Jean de Baïf, 75205 Paris, France, [‡]Laboratoire Interdisciplinaire Carnot de Bourgogne, CNRS UMR 5209, Université de Bourgogne, 9 Avenue Alain Savary, Dijon, France, and [§]Interfaces, Traitements, Organisations et Dynamique des Systèmes, Université Paris7-Denis Diderot, UMR 7086, Bâtiment Lavoisier, 15 rue Jean de Baïf, 75205 Paris, France

ABSTRACT In the present work, the combination of chemical immobilization with electron beam lithography enables the production of sensitive and reproducible SERS-active areas composed of stochastic arrangements of gold nanoparticles. The number of nanoparticles was varied from 2 to 500. Thereby a systematic analysis of these SERS-active areas allows us to study SERS efficiency as a function of the number of nanoparticles. We found that the experimental parameters are critical, in particular the size of the SERS-active area must be comparable to the effective area of excitation to obtained reproducible SERS measurements. The sensitivity has also been studied by deducing the number of NPs that generate the enhancement. With this approach we demonstrates that the maximum enhancement, the best sensitivity, is obtained with the smallest number of nanoparticles that is resonant at a given excitation wavelength.

KEYWORDS: average and single molecule SERS · surface plasmon resonance · surface functionalization · templated synthesis · gold nanoparticles · repeatability · sensitivity

Over the past decade, there has been an increased interest in finding new methods and devices that provide easy, highly reproducible, and ultrasensitive nanosensors to detect small amounts of molecules.[1−8] Specifications on such nanosensors deal with three different concepts: sensitivity, repeatability, and selectivity. Surface-enhanced Raman scattering (SERS) is already considered as a highly selective technique in the sense that the signal detected is the vibrational signature of a specific molecule. In this respect, during the last years intense efforts were invested in producing nanostructured substrates for SERS applications.[9−18] The properties of the metallic structures are modified compared to the bulk, inducing a modification of the optical response related to the effective coupling of the incident photons to the conduction electrons (localized surface plasmon). When a near field coupling between nanoparticles (NPs) occurs, a large enhancement of the incident electromagnetic field in the interstice between the NPs is observed giving rise to a so-called hot-spot.

When molecules are placed in the SERS area, the enhanced electromagnetic field is strong enough to counterbalance the low cross section of Raman scattering ($\sim 10^{-30}$ cm^2).[3,5,6,9,19,20] Although the term hot-spot might not be the most appropriate, this appellation refers to an extremely small volume where enhancement factors of 10^8 or more can be achieved,[21−24] enabling thus the detection of a few molecules. SERS signal can also arise from a larger number of molecules placed in a larger volume having a moderate enhancement factor between 10^4 and 10^8;[21,22] these enhancement volumes were defined as "cold sites".[22,25] The term "enhancement sites" (ESs) was then found more suitable. A SERS-active substrate can be defined with its average value of the enhancement factor, $\langle G \rangle$, which frequently reaches 10^6 compared with molecules without a SERS substrate. $\langle G \rangle$ is an average value that represents a broad distribution of a nanoscopic enhancement factor, which is related to a distribution of cold and hot enhancement sites. When a SERS active area is excited with an incident

* Address correspondence to jeremie.margueritat@u-bourgogne.fr.

Received for review June 7, 2010 and accepted February 16, 2011.

Published online March 02, 2011
10.1021/nn103256t

laser field E_{in}, the local electrical field E_{ES} at the ES(i) is enhanced by a factor $g_i = E_{ES}/E_{in}$.[22] The average value of the enhancement factor $\langle G \rangle = (1/N_{ES})\sum_i^{N_{ES}} g_i^4$, where N_{ES} is the number of ESs distributed over all the SERS active area and g_i the local electrical field enhancement factor.

$\langle G \rangle$ depends on multiple parameters: Raman scattering cross section of the probe molecule, excitation wavelength, incident power and polarization, surface chemistry, photochemistry, and morphology of the surface.[26] This is a nonexhaustive list of parameters that can impact both sensitivity and repeatability of SERS experiments.[27] The key point for a practical use of SERS-based sensors is the development of new fabrication methods of SERS substrates enabling stable and significant Raman enhancement, $\langle G \rangle$. Highly ordered metallic nanostructures were then developed mainly by template-assisted self-assembly or electron beam lithography.[10,12−16,28−30] Those well-ordered arrays are usually constituted by a large number of ESs. The resulting SERS signal is then an average of the signals emitted by each molecules probing the distribution of the locally enhanced electromagnetic field thereby defining as "average SERS" (a-SERS) experiments.[26,29] Recent SERS studies are mainly oriented toward the ability of SERS to approach single molecule detection, that is "single molecule SERS" (SM-SERS) measurements using a single isolated ES.[3,5,6,9,19,20,26,29] Usually, such ESs are obtained by evaporation of a colloidal solution of NPs leading to a stochastic arrangement of particles over the substrate which is therefore extremely difficult to replicate. On the other hand, it is fairly easy to reproducibly mass-fabricate localized ESs with modest local enhancement factors g by standard electron-beam lithography. Despite the lack of sensitivity for single molecule detection, those nanostructures can be duplicated easily on a chip ensuring a good repeatability of the signals required for reproducible measurements but lacking the sensitivity for "single molecule SERS".

In this work, we combine e-beam lithography and chemical immobilization in order to control the number of NPs attached at a predefined location. On a single substrate it is then possible to compare the enhancement factor $\langle G \rangle$ in a-SERS and SM-SERS regime by varying the number of NPs. The compromise between sensitivity and repeatability will thus allow to define the best conditions to design an efficient SERS detector.

RESULTS AND DISCUSSION

The study presented here is based on the combination of two fabrication methods: the chemical immobilization of colloidal NPs on a templated substrate patterned by electron-beam lithography. The procedure is illustrated in Figure 1. After e-beam lithography, indium tin oxide (ITO) square areas were functionalized

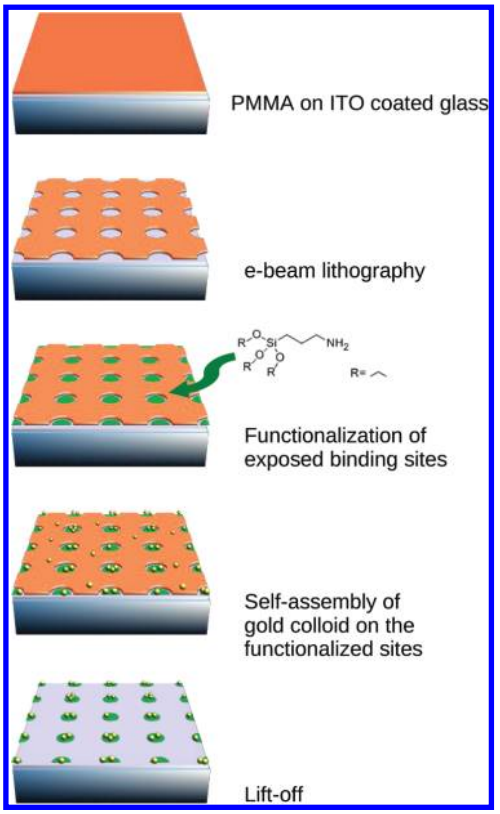

Figure 1. Schematics for the self-assembly template-assisted method to produce predefined SERS-active regions.

using 3-aminopropyltriethoxysilane (APTES). The silane termination of this molecule binds covalently to the hydroxyl sites of the ITO surface. The obtained layer of APTES is positively charged and binds electrostatically to the NPs negatively charged due to the presence of the citrate capping layer. Then the remaining resin (poly methylmethacrylate (PMMA)), used as template, is lifted off. This procedure is described with more details in the Methods section. The arrangement of the NPs provides generation of ESs with large enhancement factors, while templating offers a deterministic location of the SERS-active areas. Our substrates are thus constituted of predefined square arrays filled with a random assembly of gold NPs.

Figure 2 shows a low magnification SEM image of an array of $1 \times 1\ \mu m^2$ square patterns. It demonstrates the good control achieved during the process since the colloidal NPs are only immobilized onto the position defined by the electron beam lithography template. Moreover, since repeatability is a key parameter for sensing application, the robustness of the immobilization was tested against different treatments. Exposure to soap, trichloroethylene in ultrasonic bath, or oxygen plasma cleaner did not have any measurable effect on the integrity of the arrays. To study and compare the influence on the number of ESs inside these arrays, the area of the square was systematically reduced from 1×1 down to $0.1 \times 0.1\ \mu m^2$ to limit the number of particles located inside the defined areas from hundreds to few

as shown in Figure 3a−h. The colloidal NPs are randomly distributed onto the surface, and a large variety of arrangements and interparticle distances are observed.

Figure 3i shows a confocal intensity map recorded with an avalanche photodiode (APD) placed behind a bandpass notch filter as described in the Methods section. The signal measured is the total intensity integrated over all the spectral window defined by the notch filter. The probe molecule used here was methylene blue and the deposition process is given in the Methods section. The spectral response is shown in the SERS spectra of methylene blue plotted in Figure 4a to demonstrate that the signal is indeed due to the presence of the probe molecules. Both spectra have been acquired on a 0.15 × 0.15 (red curve) and a 1 × 1 μm^2 square (black curve), respectively, using 532 nm wavelength. No Raman spectra were acquired on areas without NPs. The same behaviors were observed with 633 and 785 nm and are not shown here. Rayleigh scattering of each structures was investigated using a dark field setup in order to compare the enhancement properties of the structures as a function of the excitation wavelength. Figure 4b shows how the surface plasmon resonance is broadened and red-shifted as the number of NPs inside the active-area increases. Both, broadening and red-shift of the plasmon resonance reveal that interactions between NPs are taking place.[31−36]

The surface coverage of NPs was estimated by plotting the number of NPs as a function of the size of the active area (Figure 5). The number of NPs is

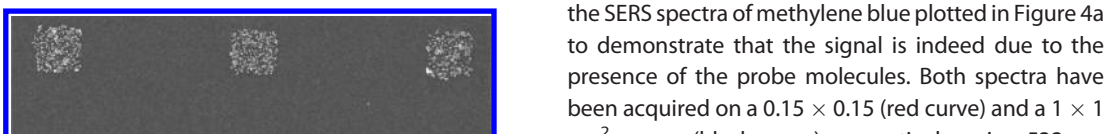

Figure 2. SEM image of an array of SERS-active areas fabricated by a random deposition of gold NPs in predefined areas. The array parameter is 5 μm and a square size of 1 × 1 μm^2.

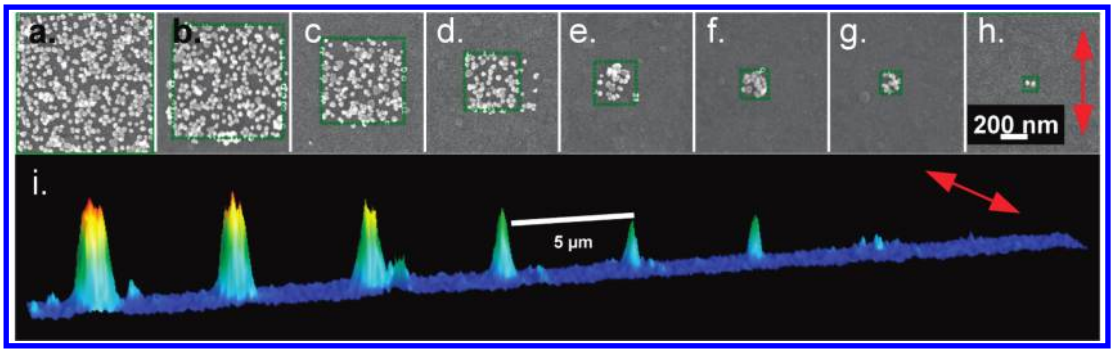

Figure 3. SEM images of colloidal arrangements obtained for different sizes of the square pattern: (a) 1 × 1 μm^2, (b) 0.8 × 0.8, (c) 0.6 × 0.6, (d) 0.4 × 0.4^2, (e) 0.3 × 0.3, (f) 0.2 × 0.2, (g) 0.15 × 0.15, and (h) 0.1 × 0.1 μm^2. (i) Confocal intensity map of the SERS signal emitted from methylene blue molecule obtained on the areas defined in panels a−h recorded using an avalanche photodiode (APD). The excitation wavelength is 532 nm. The red arrows represent the polarization as it was fixed during the experiments.

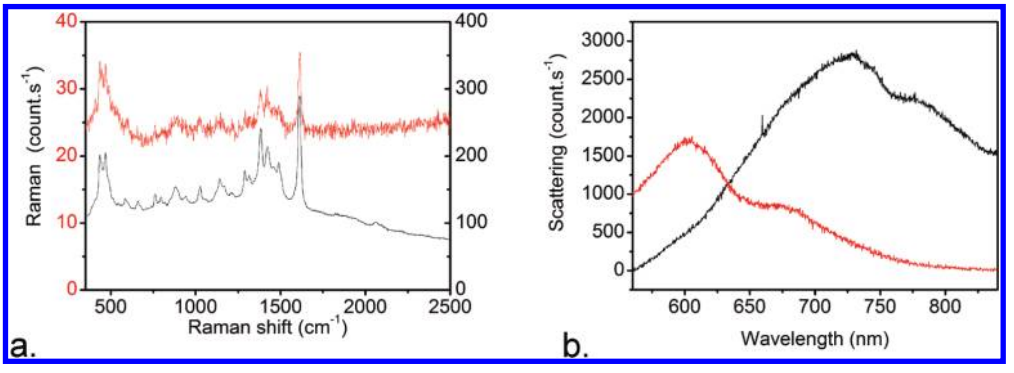

Figure 4. (a) SERS spectra of 0.15 × 0.15 (red curve and scale) and 1 × 1 μm^2 (black curve and scale). Both spectra were obtained using 532 nm laser line. (b) Scattering spectra of 0.15 × 0.15 (red curve) and 1 × 1 μm^2 (black curve).

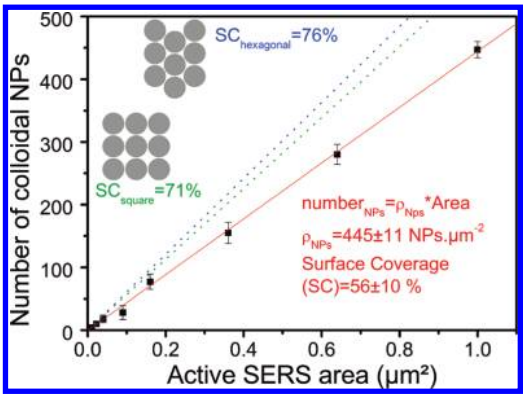

Figure 5. Number of NPs as a function of the size of SERS-active areas. The red line is a fit of the experimental data. The green and blue dashed curves correspond to cubic and hexagonal arrangements of 40 nm colloidal NPs separated by 2 nm, respectively.

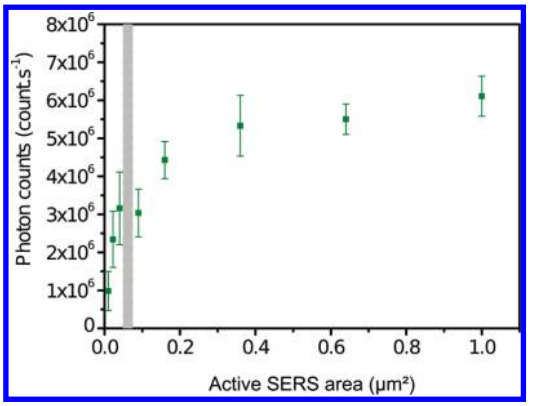

Figure 6. Photon counts as a function of the size of the SERS-active area. The error bars are the standard deviation estimated over 8 SERS-active areas of each type. The gray band corresponds to the effective area of excitation. The lower values were determined using the point spread function[38] (described in the Methods section) while the higher value was calculated using the Rayleigh criterion.

linearly dependent on the size of the area. Considering a NP diameter of 40 ± 3 nm, we deduce a surface coverage of 56 ± 10% that can be compared to an ideal coverage for a square (71%) or hexagonal (76%) arrangement of 40 nm NPs separated by 2 nm (average thickness of citrate capping[37]). The 20% difference in the surface coverage can be explained by the inhomogeneous functionalization of the squares by the APTES layer. First, since the ITO surface was not treated prior to electron beam lithography processing, the OH^- binding sites may not cover the whole surface. Second, the amine groups of the APTES might bind with the hydroxil binding sites, leading to a competition between amine and silane to bind to the surface. Both effects result in an inhomogeneous distribution of APTES onto the surface which explains the distribution of the NPs onto the surface. It is also worth noting that few NPs can attach on top of others leading to 3-dimensional arrangements. Two phenomena may lead to these arrangements: redeposition of a few NPs that were not strongly bond to the surface during the lift-off process or aggregation in solution. The latter is attenuated by placing the substrate on top of the colloidal solution as described in the Methods section. However, these 3D arrangements correspond to less than 5% of the active area, and it sounds reasonable to consider that NPs are organized in the plane of the substrate.

Figure 6 shows how the photon counts vary as a function of the SERS-active area excited at 532 nm. The photon counts were determined using the confocal intensity maps of each structure. For the smallest structures (from 0.1 × 0.1 to 0.3 × 0.3 μm^2) the photon counts were measured on the pixel corresponding to the maximum signal. For larger areas the photon counts were averaged over the pixels that define the structure. This operation was repeated for eight structures and the final photon counts represented in Figure 6 were averaged defining thus the error bars. Figure 6 shows an exponential increase in the photon counts when increasing areas before reaching a plateau where the area is larger than 0.3 μm^2. The lowest photon counts correspond to a few NPs such as a dimer (Figure 3i), when only one ES is active. In this case, the number of probe molecules n that feel the enhancement is small, and we are close to the SM-SERS regime. As the number of NPs increases, the likelihood of probing more ESs necessarily increases. As a result, the intensity increases since all the molecules present inside each ESs within our detection volume contribute to the measured signal. In other words, the measured photon counts, P_{counts}, can be defined as follows:

$$P_{counts} \propto \sum_{i}^{N_{ES}} n_i g_i^4 = n_{tot}\langle G \rangle \qquad (1)$$

where $n_{tot} = \sum_i^{N_{ES}} n_i$ is the total number of probe molecules sensing enhancement.

Within eq 1, the photon counts increase with the size of the SERS-active area since n_{tot} will necessarily increase. However, a saturation is observed in Figure 6. This saturation has two possible origins. The number of ESs increases with the number of NPs, and thus the number of molecules n_{tot}. $\langle G \rangle$ then decreases as the number of NPs increases due to near field interactions. This implies that for large areas the $\langle G \rangle$ will be low, in clear disagreement with the observations recorded in the literature.[22] The other possibility is setup-dependent and is strongly correlated to the area of excitation. The cross-section of the confocal spot of our setup at 532 nm has been estimated to be 175 ± 25 nm by determining the point spread function[38] (see Methods section). From this value we can deduce an effective area of excitation[21] of ~0.05 μm^2. We extrapolated this value to determine the surface of the excitation area at 633 and 785 nm (see Methods section). The gray band in Figure 6 corresponds to the effective area of

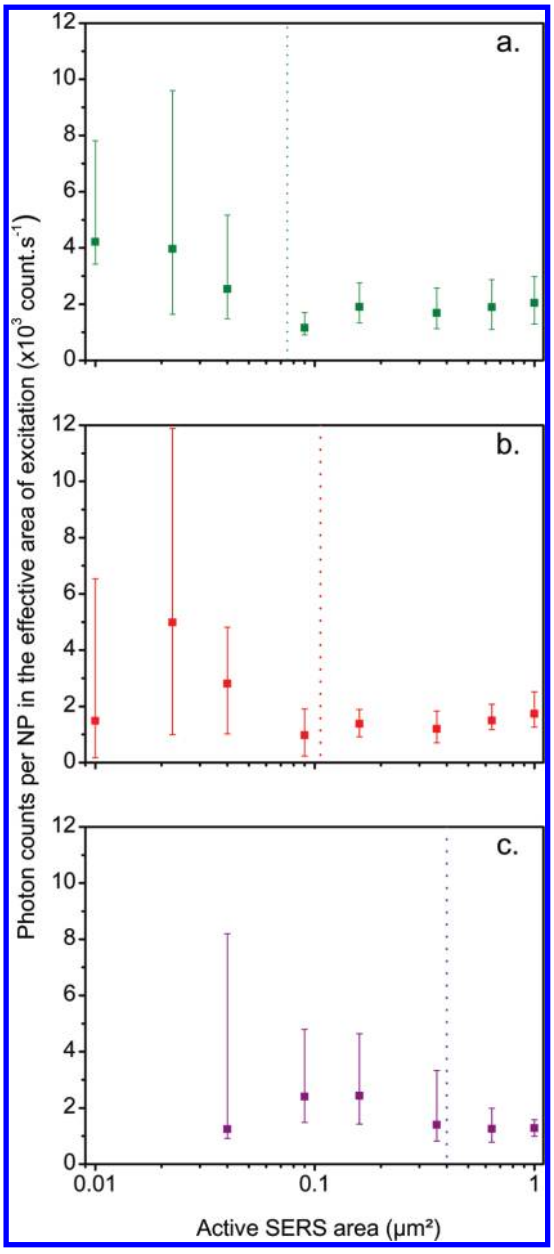

Figure 7. Photon counts per NPs as a function of the size of the SERS-active area (logarithmic scale), for (a) 532 (green), (b) 633 (red), and (c) 785 nm (purple). The error bars represent the minimum and maximum values obtained over eight structures of each type. At 785 nm, no SERS was observed for the two smaller areas. (Reminder: the intensities are not comparable). The dotted lines indicate the effective surface area[21] calculated by the Rayleigh criterion for each wavelength.

excitation, the lower value (0.05 μm^2) determined experimentally and the higher value (0.075 μm^2) calculated using the Rayleigh criterion. This implies that P_{counts} measured originates from the structures that are excited inside the effective area of excitation. In other words, when the SERS-active areas become larger than the excitation area N_{ES} excited is limited, explaining thus the saturation observed. This latter effect is dominant and therefore it is not possible to conclude about the behavior of $\langle G \rangle$.

To investigate the behavior of $\langle G \rangle$ it is interesting to compare the photon counts measured with the real number of NPs excited. This is shown in Figure 7 at three different wavelengths. Note that for experimental reasons, the intensities at the three wavelengths cannot be compared, only the shapes of the curves are informative. Indeed, methylene blue is resonant at 633 nm, and the plasmon damping is significant at 532 nm.[39,40] The maximum numbers of NPs that are contained in the effective area of excitation (Methods section) are ~22, ~47, and ~178, at 532, 633, and 785 nm excitation wavelength, respectively.

Let us first consider the smallest area where only one ES is activated (dimer Figure 3h). Two different surface plasmon resonances, corresponding to the collective oscillations of the free electrons along the short and long axis of the dimer, transverse and longitudinal mode, respectively, are excited in the range 520−540 and 580−630 nm depending on the interstitial distances.[32,41] The ES in the interstice between the NPs is excited when the polarization state is parallel to the long axis of the dimer and g is maximum when the longitudinal surface plasmon is excited close to its resonance.[41] At 532 nm, the excitation is far from the resonance of the longitudinal surface plasmon and closer to the transverse mode. Altough we do not expect a large enhancement value at 532 nm, the surface plasmon field is still strong enough to induce a measurable SERS signal whatever the orientation of the dimer toward the polarization. For these experiments the polarization direction was maintained constant, and thus only the orientations of the structures induce changes in the measured signal. The maximum intensity is observed for the smallest SERS-active area (Figure 7a). At 632 nm excitation wavelength, the largest electromagnetic enhancement is located in the gap of the dimer and thus is extremely sensitive to the polarization state as the transverse plasmon cannot be excited. In Figure 7b, the maximum photon counts is obtained for a SERS-active area of 0.15 × 0.15 μm^2, corresponding to approximately 10 NPs. Since the NPs are randomly attached onto the surface, it is more likely to obtain a dimer with the appropriate orientation (parallel to the polarization state). Out of resonance, for example at 785 nm, only dimers having very short interstitial distance can be excited,[32] which is less probable in our case due to the presence of the citrate. When increasing N_{ES}, the surface plasmon broadens and its resonance shifts to higher wavelengths as shown in Figure 4b. SERS response at 785 nm is then maximum for the largest area enclosing at least 40 excited NPs. This interpretation indicates that the maximum of the photon counts corresponds to the highest enhancement, $\langle G \rangle_{max}$, which is highly dependent on the plasmonic properties of the structure and thus on the excitation wavelength.

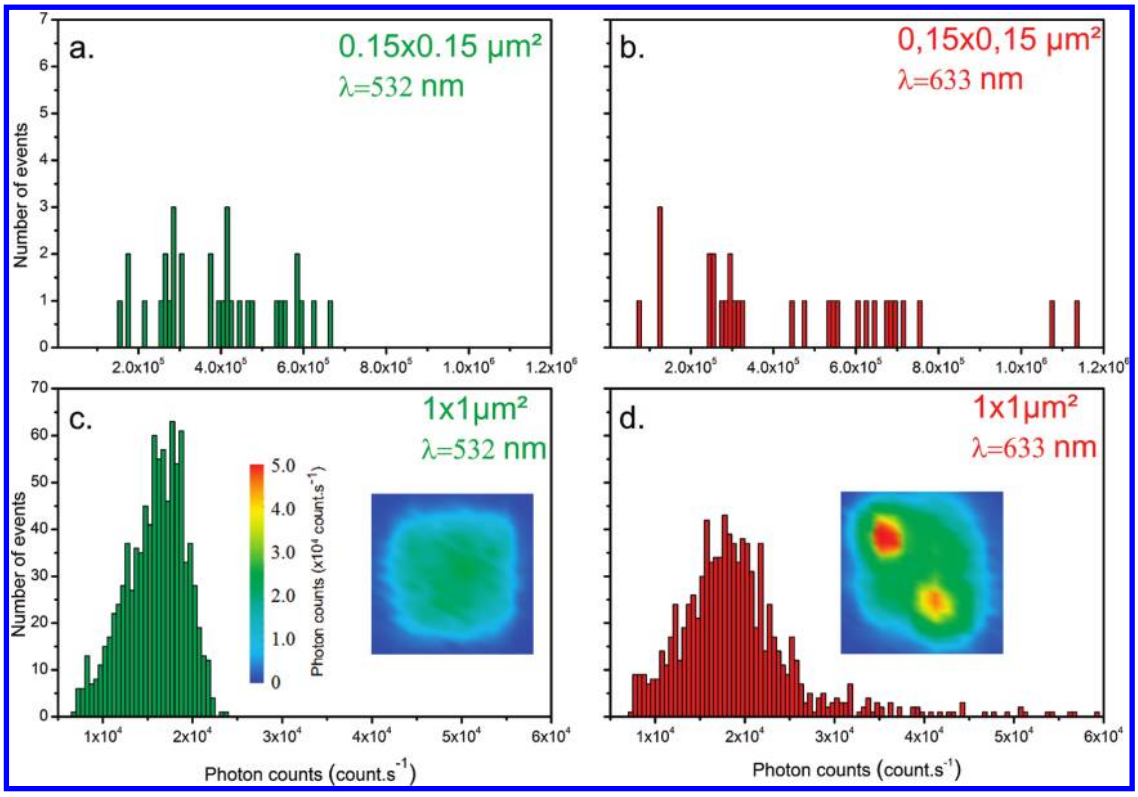

Figure 8. (a, b) Intensity distribution for functionalized area of 0.15 × 0.15 μm^2 using 532 and 633 nm excitation wavelength, respectively. (c,d) Intensity distribution for functionalized area of 1 × 1 μm^2 using 532 and 633 nm excitation wavelength, respectively. The insets in panels c and d are the confocal intensity maps at 532 and 633 nm (same scale, 1.2 × 1.2 μm^2).

In all graphs of Figure 7 the maximum of the photon counts per NPs decreases with the number of NPs and reaches a minimum value for larger SERS active area. This is unexpected since N_{ES} and n_{tot} increase. From eq 1, we deduce that g_i and thus $\langle G \rangle$ might decrease when N_{ES} increases. This effect was already predicted theoretically for different types of NPs arrangements.[31,33,42] In particular Stout *et al.*[31] shows that the maximum local enhanced field generated by five aligned NPs of silver is approximately 4 times smaller than for a dimer. In our case, the minimum of the photon counts, and thus $\langle G \rangle_{min}$, is obtained approximately for 40 NPs at 532 and 633 nm, and 160 NPs at 785 nm, corresponding approximately to the effective area of excitation. When this area is full of NPs (right side of Figure 7) the photon counts remains constant; n_{tot} and N_{ES} are constant and maximum implying that $\langle G \rangle$ tends to its minimum value $\langle G \rangle_{min}$. It is then possible to deduce the ratio between the maximum and the minimum of the photon counts that is proportional to $\langle G \rangle_{max}/\langle G \rangle_{min}$. We obtain 3.5, 5, and 2 for 532, 633, and 785 nm excitation wavelength, respectively. These values are comparable with the results obtained by Stout *et al.*[31] Although these ratios cannot be compared among wavelengths in our experiment due to the resonant probe molecules, it is worth noting that the maximum is observed at 633 nm, that is, in the resonant SERS configuration. Finally in all cases the sensitivity is reduced as N_{ES} increases. We have so far discussed about the behavior of $\langle G \rangle$ as a function of the SERS active area, and it is now interesting to discuss the repeatability of these measurements.

In this last part, we compare the statistical distributions of the intensity per NPs in large and small areas (Figure 8) at two excitation wavelengths. At this stage we have to recall that only the behaviors measured at each wavelength are comparable, and not their intensities. With few ESs (small area), the photon counts are randomly distributed (Figure 8a,b), reaching high value at rare places (>10^6 count s^{-1}). The equiprobability suggests then a bad repeatability. On the opposite side, for larger active area the intensity is normally distributed (Figure 8c,d). The high N_{ES} favors the repeatability: more molecules can feel the same enhancement $\langle G \rangle_{min}$. However, the distribution of the photon counts in a large SERS-active area (Figure 8b) can change at different excitation wavelengths. At 532 nm, the distribution of photon counts is relatively well centered at 1.5 × 10^4 count s^{-1}. The confocal map shows a quasi-constant signal over the square area: single NPs are resonantly excited. At 633 nm, a long tail is observed in the distribution. Intensities higher than 2 × 10^4 count s^{-1} demonstrate the presence of ESs with high enhancement factors among ESs having low enhancement factors. This was also clearly observed in the confocal intensity maps at λ = 633 nm. This is

again related to the likelihood of excited resonant structures that are generated by the stochastic arrangements of the NPs.

CONCLUSIONS

Our fabrication technique allowed us to vary the number of colloidal NPs in a determined position and area, with high control and repeatability. This gives us the opportunity to study the SERS response of methylene blue molecules deposited on our substrate as a function of the number of NPs. It was found that it is not necessary to build a large SERS active area since the measurements are limited by the effective area of excitation. Moreover the photon counts measured must be reported to the number of NPs to deduce the real enhancement of the SERS-active area. Using this method we demonstrate that the maximum photon counts per NP are obtained for the smallest number of NPs that is resonant with the excitation wavelength. This case corresponds to the higher sensitivity and the lower repeatability. On the opposite, the photon counts measured on larger structures are more reproducible, but with a sensitivity 5 times less (at 633 nm). Finally, the choice of a stochastic arrangement of NPs was discussed in terms of the distribution of the uncontrolled local enhancement factor, g_i. SERS areas of random active enhancement g_i might be very robust against experimental parameters (polarization, wavelength, *etc*...) thereby providing significant advantages for probing the SERS activity of unknown nonresonant molecules. Moreover, controlling the size and position of the SERS-active area allows us to optimize the repeatability of experiments whatever the distribution of g_i, keeping in mind that the SERS-active area should be comparable or slightly smaller than the effective area of excitation defined by the confocal spot.

METHODS

Template Assisted Self-Assembly. The multistep procedure consists in a combination of two fabrication techniques. In a first step, an array of squares (5 μm period) is created in a poly(methyl methacrylate) (PMMA) film on top of 50 nm thin indium tin oxide (ITO) film using electron beam lithography followed by a development of the resist. The development procedure exposes the ITO surface which will be subsequently functionalized by dipping the substrate in a 5% solution of 3-aminopropyltriethoxysilane (APTES) in ethanol during 30 min. The ITO surface naturally exhibits hydroxil (OH^-) sites allowing the silane termination of the APTES to bind with the ITO surface. A positively charged monolayer is thus produced by the amine compound. This template is then placed on top of a drop of colloidal suspension of gold NPs, sufficiently large to avoid total evaporation for 12 h. We experienced that this process reduces the deposition of large clusters of NPs, that can be present in the colloidal solution, on the surface. The NPs were prepared according to the Frens method.[43] Since their surface is negatively charged by the presence of a citrate monolayer, the self-assembly of the colloidal NPs is mainly governed by electrostatic interactions.[44] The colloidal suspension contains spherical NPs with an average diameter of 40 $\pm$ 3 nm. However, few triangles resulting from the colloidal synthesis method are also present, but their number is negligible (about 1 triangle for 70 spheres). Finally, after rinsing the substrate several times with deionized water the remaining PMMA is lifted off using acetone and by ultrasonic agitation. All colloidal NPs incidentally deposited on top of the PMMA layer as well as those that are weakly attached to the surface are thus removed. The morphology and structure of the SERS-active areas obtained were observed by scanning electron microscopy (SEM) at 20 kV.

SERS Measurements. To demonstrate the SERS efficiency of our structures, a drop (100 μL) of a 10^{-6} mol·L^{-1} solution of methylene blue in isopropyl alcohol was spin coated at 2000 rpm onto the substrate. SERS mappings were performed using two different confocal setups at excitation wavelengths of 532 and 633 nm (setup 1) and 785 nm (setup 2).

Setup 1: (532 and 633 nm) The sample was moved using a piezoelectric *XY* translation stage to perform two-dimensional scanning (*XY* step size fixed to 80 nm). The incident laser excitation is focused using a $\times$100 oil-immersion objective (NA = 1.49). The backscattered signal is filtered using a band-pass notch filter. The signal was monitored either by an avalanche photodiode (APD) or by a spectrometer equipped with a thermo-electric cooled CCD. The time response of the APD was 1 ms. The confocal aperture is defined by the size of the APD detector, that is, 150 μm. The acquisition time for the spectrometer was 20 s using 600 line per millimeters grating. The spectrometer was essentially used to confirm that the signal measured with the APD was due to the enhanced Raman signature of methylene blue.

Setup 2: (785 nm) We use a commercial confocal Raman spectrometer coupled with a 785 nm excitation wavelength. The Labram HR (Jobin−Yvon) spectrometer is equipped with a thermo-electric cooled CCD and motorized *XY* displacement stage. The objective was a conventional $\times$100 in air (NA = 0.95), and a band-pass notch filter was placed before the pinhole aperture fixed at 150 μm. The grating (1800 lines per millimeters) was either used as mirror (0th order) for the total intensity map acquisition (1 ms per point), or as spectrometer to check the reality of the Raman signal (acquisition time: 20 s per spectrum). For *XY* mapping, the step size was fixed to 100 nm.

The optical power was maintained as low as possible in both setups to avoid photobleaching ($\leq$50 μW), and the light was linearly polarized in all experiments(Figure 3).

Point-Spread Function. The point-spread function of setup 1 was determined at 532 nm using the method described by Novotny and Hecht.[38] A solution of fluoro-spheres of 60 nm diameter (excitation 530 nm; emission 560 nm) at low concentration was spin-coated onto a glass surface in order to obtain well separated nanospheres. When a single object was localized, the focus (z) was adjusted by maximizing the detected intensity. Then, multiple lateral cross section scans were acquired with x step of 15 nm and acquisition time of 5 ms per point. We thus obtained the intensity profile as a function of x, which can be fitted by a Gaussian intensity profile:

$$I(x, z = 0) = I_0 \exp\left(-\frac{2x^2}{\omega(z = 0)^2}\right) \quad (2)$$

where $\omega(z = 0) = \omega_0$ is the waist of the Gaussian beam. In our experiment at 532 nm ω_0 = 175 $\pm$ 5 nm. This value was compared to the diameter of the Airy disk which can be approximated by the Rayleigh criterion as follows:

$$D_{\text{airy}} \approx \frac{1.22\lambda_{\text{exc}}}{2 \times \text{NA}} \quad (3)$$

In our experiment at λ_{exc} = 532 nm with NA = 1.49, $D_{\text{airy}} \approx$ 218 nm. The experimental value is lower than the estimated

theoretical value; however, the Rayleigh criterion gives a good approximation. We have thus calculated this value at 633 nm (NA = 1.49) and 785 nm (NA = 0.95): $D_{airy}^{633} \approx 260$ nm and $D_{airy}^{785} \approx 504$ nm.

The effective surface area of the Gaussian excitation,[21] $A_{eff} = (\pi\omega_0^2)/2$ was determined at each wavelength. $A_{eff}^{532} \approx 0.050\ \mu m^2$, $A_{eff}^{633} \approx 0.105\ \mu m^2$, and $A_{eff}^{785} \approx 0.400\ \mu m^2$.

Acknowledgment. This work was supported by the Contracts ANTARES 007-NANO-006 and DGA REI 2007-34-026. The research leading to these results has received funding from European Community's Seventh Framework Programme (FP7-ICT-2009-4) (SPEDOC) under Grant agreement No. 248835.

REFERENCES AND NOTES

1. Kneipp, K.;Wang, Y.; Kneipp, H.; Perelman, L. T.; Itzkan, I.; Dasari, R. R.; Feld, M. S. Single Molecule Detection Using Surface-Enhanced Raman Scattering (SERS). *Phys. Rev. Lett.* 1997, *78*, 1667−1670.
2. Le Ru, E. C.; Meyer, M.; Etchegoin, P. G. Proof of Single-Molecule Sensitivity in Surface-Enhanced Raman Scattering (SERS) by Means of a Two-Analyte Technique. *J. Phys. Chem. B* **2006,** *110*, 1944–1948.
3. Etchegoin, P. G.; Le Ru, E. C. A Perspective on Single Molecule SERS: Current Status and Future Challenges. *Phys. Chem. Chem. Phys.* **2008,** *10*, 6079–6089.
4. Nie, S.; Emory, S. R. Probing Single Molecules and Single Nanoparticles by Surface-Enhanced Raman Scattering. *Science* **1997,** *275*, 1102–1106.
5. Svedberg, F.; Li, Z.; Xu, H.; Kall, M. Creating Hot Nanoparticle Pairs for Surface-Enhanced Raman Spectroscopy through Optical Manipulation. *Nano Lett.* **2006,** *6*, 2639–2641.
6. Camden, J. P.; Dieringer, J. A.; Wang, Y.; Masiello, D. J.; Marks, L. D.; Schatz, G. C.; Van Duyne, R. P. Probing the Structure of Single-Molecule Surface-Enhanced Raman Scattering Hot Spots. *J. Am. Chem. Soc.* **2008,** *130*, 12616–12617.
7. Haran, G. Single-Molecule Raman Spectroscopy: A Probe of Surface Dynamics and Plasmonic Fields. *Acc. Chem. Res.* **2010,** *43*, 1135.
8. Lombardi, J. R.; Birke, R. L. A Unified View of Surface-Enhanced Raman Scattering. *Acc. Chem. Res.* **2008,** *42*, 734–742.
9. Camden, J. P.; Dieringer, J. A.; Zhao, J.; Van Duyne, R. P. Controlled Plasmonic Nanostructures for Surface-Enhanced Spectroscopy and Sensing. *Acc. Chem. Res.* **2008,** *41*, 1653–1661.
10. Gopinath, A.; Boriskina, S. V.; Premasiri, W. R.; Ziegler, L.; Reinhard, B. M.; Dal Negro, L. Plasmonic Nanogalaxies: Multiscale Aperiodic Arrays for Surface-Enhanced Raman Sensing. *Nano Lett.* **2009,** *9*, 3922–3929.
11. Homola, J. Surface Plasmon Resonance Sensors: Review. *Sensor Actuat. B* **1999,** *54*, 3–15.
12. Malic, L.; Cui, B.; Veres, T.; Tabrizian, M. Enhanced Surface Plasmon Resonance Imaging Detection of DNA Hybridization on Periodic Gold Nanoposts. *Opt. Lett.* **2007,** *32*, 3092–3094.
13. Sato, Y.; Hosokawa, K.; Maeda, M. Detection of Non-Cross-Linking Interaction Between DNA-Modified Gold Nanoparticles and a DNA-Modified Flat Gold Surface Using Surface Plasmon Resonance Imaging on a Microchip. *Colloids Surf., B* **2008,** *62*, 71–76.
14. Stadler, B.; Solak, H. H.; Frerker, S.; Bonroy, K.; Frederix, F.; Voros, J.; Grandin, H. M. Nanopatterning of Gold Colloids for Label-Free Biosensing. *Nanotechnology* **2007,** *18*, 155306.
15. Anker, J. N.; Hall, W. P.; Lyandres, O.; Shah, N. C.; Zhao, J.; van Duyne, R. P. Biosensing with Plasmonic Nanosensors. *Nat. Mater.* **2008,** *7*, 442–453.
16. Cerf, A.; Molnár, G.; Vieu, C. Novel Approach for the Assembly of Highly Efficient SERS Substrates. *ACS Appl. Mater. Interfaces* **2009,** *1*, 2544–2550.
17. Rycenga, M.; Wang, Z.; Gordon, E.; Cobley, C. M.; Schwartz, A. G.; Lo, C. S.; Xia, Y. Probing the Photothermal Effect of Gold-Based Nanocages with Surface-Enhanced Raman Scattering (SERS). *Angew. Chem. Int.* **2009,** *48*, 9924–9927.
18. Rycenga, M.; Hou, K. K.; Cobley, C. M.; Schwartz, A. G.; Camargo, P. H. C.; Xia, Y. Probing the Surface-Enhanced Raman Scattering Properties of Au−Ag Nanocages at Two Different Excitation Wavelengths. *Phys. Chem. Chem. Phys.* **2009,** *11*, 5903–5908.
19. Li, W.; Camargo, P. H. C.; Lu, X.; Xia, Y. Dimers of Silver Nanospheres: Facile Synthesis and Their Use as Hot Spots for Surface-Enhanced Raman Scattering. *Nano Lett.* **2009,** *9*, 485–490.
20. Jain, P.; Huang, X.; El-Sayed, I.; El-Sayed, M. Review of Some Interesting Surface Plasmon Resonance-Enhanced Properties of Noble Metal Nanoparticles and Their Applications to Biosystems. *Plasmonics* **2007,** *2*, 107–118.
21. Le Ru, E. C.; Blackie, E.; Meyer, M.; Etchegoin, P. G. Surface-Enhanced Raman Scattering Enhancement Factors: A Comprehensive Study. *J. Phys. Chem. C* **2007,** *111*, 13794–13803.
22. Fang, Y.; Seong, N.-H.; Dlott, D. D. Measurement of the Distribution of Site Enhancements in Surface-Enhanced Raman Scattering. *Science* **2008,** *321*, 388.
23. Krug, J. T.; Wang, G. D.; Emory, S. R.; Nie, S. Efficient Raman Enhancement and Intermittent Light Emission Observed in Single Gold Nanocrystals. *J. Am. Chem. Soc.* **1999,** *121*, 9208–9214.
24. Dieringer, J. A.; Lettan, R. B., II; Scheidt, K. A.; Van Duyne, R. P. A Frequency Domain Existence Proof af Single-Molecule Surface-Enhanced Raman Spectroscopy. *J. Am. Chem. Soc.* **2007,** *129*, 204701.
25. Le Ru, E. C.; Etchegoin, P. G.; Meyer, M. Enhancement Factor Distribution around a Single Surface-Enhanced Raman Scattering Hot Spot and Its Relation to Single Molecule Detection. *J. Chem. Phys.* 2006, *125*, 204701+.
26. Le Ru, E. C.; Etchegoin, P. G. *Principles of Surface-Enhanced Raman Spectroscopy and Related Plasmonic E*ects*; Elsevier: Oxford, U.K., 2009.
27. Nathan, M. J. Concluding Remarks: Surface-Enhanced Raman Scattering. *Faraday Discuss.* **2006,** *132*, 321–328.
28. Su, P. Y.; Hu, J. C.; Cheng, S. L.; Chen, L. J.; Liang, J. M. Self-Assembled Hexagonal Au Particle Networks on Silicon from Au Nanoparticle Solution. *Appl. Phys. Lett.* **2004,** *84*, 3480.
29. Ko, H.; Singamaneni, S.; Tsukruk, V. V. Nanostructured Surfaces and Assemblies as SERS Media. *Small* **2008,** *4*, 1576–1599.
30. Rycenga, M.; Camargo, P. H. C.; Xia, Y. Template-Assisted Self Assembly: A Versatile Approach to Complex Micro- and Nanostructures. *Soft Matter* **2009,** *5*, 1129–1136.
31. Stout, B.; Auger, J. C.; Devilez, A. Recursive T Matrix Algorithm for Resonant Multiple Scattering: Applications to Localized Plasmon Excitations. *J. Opt. Soc. Am. A* **2008,** *25*, 2549.
32. Ringler, M.; Schwemer, A.; Wunderlich, M.; Nichtl, A.; Kurzinger, K.; Klar, T.; Feldmann, J. Shaping Emission Spectra of Fluorescent Molecules with Single Plasmonic Nanoresonators. *Phys. Rev. Lett.* **2008,** *100*, 203002.
33. Xu, H. Calculation of the Near Field of Aggregates of Arbitrary Spheres. *J. Opt. Soc. Am.* **2004,** *21*, 804.
34. Jiang, J.; Bosnik, K.; Maillard, M.; Brus, L. Single Molecule Raman Spectroscopy at the Junctions of Large Ag Nanocrystals. *J. Phys. Chem. B* **2003,** *107*, 9964–9972.
35. Li, Z.; Shegai, T.; Haran, G.; Xu, H. Multiple-Particle Nanoantennas for Enormous Enhancement and Polarization Control of Light Emission. *ACS Nano* **2009,** *3*, 637–642.
36. Bouhelier, A.; Bachelot, R.; Im, J. S.; Wiederrecht, G. P.; Lerondel, G.; Kostcheev, S.; Royer, P. Electromagnetic Interactions in Plasmonic Nanoparticle Arrays. *J. Phys. Chem. B* **2005,** *109*, 3195–3198.
37. Wanner, M.; Gerthsen, D.; Jester, S.; Sarkar, B.; Schwederski, B. Treatment of Citrate-Capped Au Colloids with NaCl, NaBr, and Na_2SO_4: A TEM, EAS, and EPR Study of the Accompanying Changes. *Colloid Polym. Sci.* **2005,** *283*, 783–792.
38. Novotny, L.; Hecht, B. *Principles of Nano-Optics*; Cambridge University Press: Cambridge, U.K., 2006.

39. Sonnichesen, C.; Franzl, T.; Wilk, T.; von Plessen, G.; Feldmann, J. Drastic Reduction of Plasmon Damping in Gold Nanorods. *Phys. Rev. Lett.* **2002,** *88*, 077402.
40. Rycenga, M.; McLellan, J. M.; Xia, Y. A SERS Study of the Molecular Structure of Alkanethiol Monolayers on Ag Nanocubes in the Presence of Aqueous Glucose. *Chem. Phys. Lett.* **2008,** *463*, 166–171.
41. Tognalli, N.; Fainstein, A.; Calvo, E.; Bonazzola, C.; Pietrasanta, L.; Compoy-Quiles, M.; Etchegoin, P. G. SERS in PAH-Os and Gold Nanoparticle Self-Assembled Multilayers. *J. Chem. Phys.* **2005,** *123*, 044707.
42. Wang, Z. B.; Luk'yanchuk, B. S.; Guo, W.; Edwardson, S. P.; Whitehead, D. J.; Li, L.; Liu, Z.; Watkins, K. G. The Influences of Particle Number on Hot Spots in Strongly Coupled Metal Nanoparticles Chain. *J. Chem. Phys.* **2008,** *128*, 094705.
43. Frens, G. Controlled Nucleation for Regulation of Particle-Size in Monodisperse Gold Suspensions. *Nat. Phys. Sci.* **1973,** *241*, 20–22.
44. Helena de Araujo Nicolai, S.; Rodrigues, P. R.; Agosthino, S. M.; Rubim, J. C. Electrochemical and Spectroelectrochemical (SERS) Studies of the Reduction of Methylene Blue on a Silver Electrode. *J. Electroanal. Chem.* **2002,** *527*, 103–111.